MPI 2007 Corning Problem: Stability of Fiber Pulling July 15, 2008

J.S. Abbott (Corning), R.J. Braun (Delaware), K. Bhalerao (RPI), I. Griffiths (Oxford), M. Gratton (Duke), B. Smith (Northwestern), C.P. Please (Southampton), C. Breward (Oxford), D. Boy (Olin).

1 Introduction

The stability of fiber pulling is considered here; of particular interest in this MPI is the diameter variation of the fiber during pulling, and trying to quantify the variation of the diameter with flow and pulling conditions. The pulling of a fiber was studied at MPI 2001 [1]; the progress there was based in significant measure on P. Howell's thesis [2]. However, the stability of the solution was not considered in that study.

The stability of pulling an solid fiber has been studied before; the isothermal case includes [3, 6, 7, 4, 5] and a summary of older work, including a number of non-Newtonian models can be found in Pearson's book [8]. Studies of the nonisothermal case include [9, 10, 11] and many others; a modern review can be found in the D.Phil. thesis of Voyce [12].

More modern issues ar concerned with the dynamics of the instability. Some surveys have pointed out the variety of diameter fluctuations that can occur [13, 14, 15, 16, 17]. Stability analyses of different types suggest that fibers being pulled may be unconditionally stable [11] or chaotic [19]. The discrpancy may be explained in part by the conditions under which the modeling are done; when the pulling velocity is specified the instability, known as draw resonance occurs; when the pulling force is specified, the instability may not occur [12, 18].

Many modern studies involve fibers that do not have uniform properties in the cross section. These may include holey fibers with air inclusion (see e.g., [20, 21, 22, 23]) or different glass materials from say doping (e.g., [24]). These efforts may aim to decrease losses from signals, increase flexibility of the fiber, or both. For a modern review, see Voyce's thesis or [22], e.g.

There are two aspects that were studied. One is to try the idea of boudinage (French for sausage); stretching or compression of fluids containing viscous inclusions of different viscosity of fluid may lead to instability as is seen in geological flows and models (e.g., [25, 26, 27, 28]). In the limit of this view, the curvature from starting with a thick blank and ending with a thin fiber (necking) is neglected, and the blank is uniformly stretched in the absence of any instability. However, stretching can induce instability; a varicose instability may form with shapes that are characteristic in tension (boudinage) and compression (inverse boudinage or mullions) [25, 26]. Circular shapes may become distorted [25, 29] and initially flat layers may develop varicose or sinuous (folding) instabilities (e.g., [25, 26, 27, 28]).

In this work, we focus on varicose instability for viscous inclusions, and ignore the possibility of fold instabilities. We use the term boudinage to refer to the stretching of included viscous layers and the resulting instability that results from stretching. We hope that context will make clear the distinction between the approach to modeling as opposed to shapes obtained after instability

(boudinage *vs* mullions).

The practical idea for fibers of interest here is to have different viscosities at different initial radii, and then stretch; will instability occur in the isothermal case? In the best situation, the model has more viscous fluid at its core and at the outer radius, with a less viscous region between. This situation would model a holey region in an annulus that acts to keep light inside the fiber.

2 Estimates

We now estimate the sizes of some parameters. The fiber speed V is taken to be 25×10^{-6}m/s in the region of interest at the hot end of the fiber near the die head and $V = 25$m/s far from the blank where the fiber has effectively reached its final diameter. The length L_0 along the fiber in the region of interest is $L_0 = 2.5$m. Thus a time scale may be $L_0/V = 0.1$s. The final radius of the fiber is $R_f = 125 \times 10^{-6}$m; the initial blank radius is $R_i = 125 \times 10^{-3}$m. Let $\epsilon = R_i/L = 5 \times 10^{-4}$.

The viscosity depends on the temperature of the glass and the material. We use a minimum value of the viscosity in the range of $\mu = 10^3$ to 4×10^5Pa·s and a maximum value in the range $\mu = 10^6$ to 2×10^7Pa·s. We use a density of $\rho = 2500$kg/m^3.

Using the low speed $V = 25 \times 10^{-6}$m/s and low viscosity $\mu = 10^3$Pa·s, we approximate the conditions near the blank with the Reynolds number $\mathrm{Re} = \rho V L_0/\mu \approx 10^{-3}$. For the conditions far from the blank, we use the high speed $V = 25$m/s and low viscosity $\mu = 10^7$Pa·s, we find the Reynolds number to be $\mathrm{Re} \approx 10^{-2}$.

3 Boudinage

3.1 Formulation

In isothermal formulation of stretching of a viscous inclusion is considered; the centerline of the fluid is assumed to be straight. We nondimensionalized the governing equations with length $L_0 = 2.5m$ and pulling speed V in the axial direction (z); ϵL_0 and ϵV in radial direction. Time was scaled with The pressure was scaled with a viscous scale.

The two fluid case with an initial state of coaxial fluids with length L_0 with inner radius $a_1(z,t)$ and outer radius $a_2(z,t)$. The inner fluid (viscosity μ_1) is thus located in $0 \le r < a_1(z,t)$ and the outer fluid (viscosity μ_2) is in $a_1(z,t) < r \le a_2(z,t)$.

The nondimensional equations in the fluid i, with $i = 1, 2$, are

$$\frac{1}{r}(ru^{(i)})_{,r} + w^{(i)}_{,z} = 0, \tag{1}$$

$$\epsilon^2 \mathrm{Re}\left(w^{(i)}_{,t} + u^{(i)}w^{(i)}_{,r} + w^{(i)}w^{(i)}_{,z}\right) = \mu^{(i)}\left[\frac{1}{r}(rw^{(i)}_{,r})_{,r} + 2w^{(i)}_{,zz} + \frac{1}{r}(ru^{(i)}_{,z})\frac{\epsilon^2}{r}\right] - \epsilon^2 p^{(i)}_{,z} + \epsilon^2 \mathrm{St}, \tag{2}$$

$$\epsilon^2 \mathrm{Re}\left(u^{(i)}_{,t} + u^{(i)}u^{(i)}_{,r} + w^{(i)}u^{(i)}_{,z}\right) = \mu^{(i)}\left[\frac{1}{r}(ru^{(i)}_{,r})_{,r} + u^{(i)}_{,zz}\right] - \epsilon^2 p^{(i)}_{,z}. \tag{3}$$

Here $\mu^{(1)} = 1$, $\mu^{(2)} = \mu_{12}$. $\mathrm{St} = \rho g L_0^2/\mu/V$ is the Stokes number.

At $r = 0$, we have symmetry, $w^{(1)}_{,r} = u^{(1)} = 0$.

At the outermost radius $r = a_2(z,t)$, we have

$$a_{2,t} + w^{(2)}a_{2,z} = u^{(2)} \tag{4}$$

$$\epsilon^2 a_{2,z}(u^{(2)}_{,r} - w^{(2)}_{,z}) + \frac{1}{2}(1-\epsilon^2 a^2_{2,z})(w^{(2)}_{,r} + \epsilon^2 u^{(2)}_{,z}) = 0, \tag{5}$$

$$-p^{(2)} + \frac{2\mu}{1+\epsilon^2 a^2_{2,z}}\left[u^{(2)}_{,r} - a^2_{2,z}(w^{(2)}_{,r} + \epsilon^2 u^{(2)}_{,z}) + \epsilon^2 a^2_{2,z} w^{(2)}_{,z}\right] = -\frac{1}{\epsilon \mathrm{Ca}\sigma}\left[\frac{1+\epsilon^2(a^2_{2,z} - a_2 a_{2,zz})}{a_2(1+\epsilon^2 a^2_{2,z})^{3/2}}\right]. \tag{6}$$

These are, respectively, the kinematic, the tangential stress and the normal stress conditions. The parameter $\mathrm{Ca} = \sigma_1/(\mu^{(1)}V)$ is the capillary number based on the inner fluid and $\sigma = \sigma_2/\sigma_1$ is the surface tension ratio.

At $r = a_1(z,t)$, we continuity of the velocity components, $u^{(1)} = u^{(2)}$ and $w^{(1)} = w^{(2)}$, as well as the kinematic, the tangential stress and the normal stress conditions, respectively:

$$a_{1,t} + w^{(1)} a_{1,z} = u^{(1)} \tag{7}$$

$$\epsilon^2 a_{1,z}(u^{(2)}_{,r} - w^{(2)}_{,z}) + \frac{1}{2}(1-\epsilon^2 a^2_{1,z})(w^{(2)}_{,r} + \epsilon^2 u^{(2)}_{,z}) = \epsilon^2 a_{1,z}(u^{(1)}_{,r} - w^{(1)}_{,z}) + \frac{1}{2}(1-\epsilon^2 a^2_{1,z})(w^{(1)}_{,r} + \epsilon^2 u^{(1)}_{,z}), \tag{8}$$

$$-p^{(1)} + \frac{2\mu}{1+\epsilon^2 a^2_{1,z}}\left[u^{(1)}_{,r} - a^2_{1,z}(w^{(1)}_{,r} + \epsilon^2 u^{(1)}_{,z}) + \epsilon^2 a^2_{1,z} w^{(1)}_{,z}\right] = -p^{(2)} + \frac{2\mu}{1+\epsilon^2 a^2_{2,z}}\left[u^{(2)}_{,r} - a^2_{2,z}(w^{(2)}_{,r} + \epsilon^2 u^{(2)}_{,z}) + \epsilon^2 a^2_{2,z} w^{(2)}_{,z}\right] - \frac{1}{\epsilon \mathrm{Ca}^{(1)}}\left[\frac{1+\epsilon^2(a^2_{1,z} - a_1 a_{1,zz})}{a_1(1+\epsilon^2 a^2_{1,z})^{3/2}}\right]. \tag{9}$$

The viscosity contrast is defined as $\mu_{12} = \mu^{(2)}/\mu^{(1)}$; we note that $\mu_{12} = 1/m$, where m is the viscosity ratio used by Smith [25]. In what follows we neglect surface tension ($\mathrm{Ca}\to\infty$), inertia ($\mathrm{Re}= 0$) and gravity ($\mathrm{St}= 0$).

3.1.1 One fluid

By eliminating the outer fluid, we can recover the one-fluid case. The derivation of the evolution equations for a slender fiber have been derived many places elsewhere, e.g. [2, 22]. They are equations for the leading order axial velocity component $w_0(z,t)$ and cross-sectional area $A(z,t)$ as follows:

$$A_{,t} + (w_0 A)_{,z} = 0, \quad \text{and } (3Aw_{0,z}), z = 0. \tag{10}$$

See Howell's thesis for a derivation of a solution in this case. Note that the leading order axial velocity is independent of the radial coordinate and it was obtained at the next order (not leading order); these equations may be thought of as mass conservation and an axial force balance. We expect similar things to happen in the two fluid case.

3.1.2 Two fluids

We use a regular expansion of all dependent variables in even powers of ϵ starting from 0; e.g., $w(r,z,t) = w_0 + \epsilon^2 w_2 + \ldots$.

The leading order equations are, for the inner fluid on $0 < r < a_1(z,t)$,

$$\begin{aligned} \frac{1}{r}\left(r u_0^{(1)}\right)_{,r} + w_{0,z}^{(1)} &= 0, && (11)\\ \frac{1}{r}\left(r w_{0,r}^{(1)}\right)_{,r} &= 0, && (12)\\ -p_{0,r}^{(1)} + \left[\frac{1}{r}\left(r u_0^{(1)}\right)_{,r}\right]_{,r} &= 0. && (13) \end{aligned}$$

For the outer fluid in $a_1(z,t) < r < a_2(z,t)$, we have

$$\begin{aligned} \frac{1}{r}\left(r u_0^{(2)}\right)_{,r} + w_{0,z}^{(2)} &= 0, && (14)\\ \frac{1}{r}\left(r w_{0,r}^{(2)}\right)_{,r} &= 0, && (15)\\ -p_{0,r}^{(2)} + \mu_{12}\left[\frac{1}{r}\left(r u_0^{(1)}\right)_{,r}\right]_{,r} &= 0. && (16) \end{aligned}$$

On the interface between fluids 1 and 2 at $r = a_1(z,t)$ we have

$$\begin{aligned} a_{1,t} + w_0^{(1)} a_{1,z} &= u_0^{(1)} && (17)\\ u_0^{(1)} &= u_0^{(2)} && (18)\\ w_0^{(1)} &= w_0^{(2)} && (19)\\ w_{0,r}^{(1)} &= \mu_{12} w_{0,r}^{(2)} && (20)\\ -p_{0,r}^{(1)} + 2\left(u_{0,r}^{(1)} - a_{1,z} w_{0,r}^{(1)}\right) + p_{0,r}^{(2)} - 2\mu_{12}\left(u_{0,r}^{(2)} - a_{1,z} w_{0,r}^{(2)}\right) &= 0. && (21) \end{aligned}$$

On the outer surface at $r = a_2(z,t)$, we have

$$\begin{aligned} a_{2,t} + w_0^{(2)} a_{2,z} &= u_0^{(2)} && (22)\\ w_{0,r}^{(2)} &= 0 && (23)\\ -p_{0,r}^{(2)} + 2\mu_{12}\left(u_{0,r}^{(2)} - a_{2,z} w_{0,r}^{(2)}\right) &= 0. && (24) \end{aligned}$$

Integrating what is left of the momentum equations for each fluid shows that

$$\begin{aligned} w_0^{(1)} &= C_1(z,t)\ln r + C_2(z,t), && (25)\\ w_0^{(2)} &= C_3(z,t)\ln r + C_4(z,t). && (26) \end{aligned}$$

For the inner fluid, $C_1 = 0$ for a bounded solution; from the shear stress condition at the interface, we must have $C_3 = 0$. Thus, the leading order axial velocity in both fluids is independent of radius. We let

$$w_0^{(1)} = w_0^{(1)}(z,t) \text{ and } w_0^{(2)} = w_0^{(2)}(z,t); \quad (27)$$

then using mass conservation in each fluid, we find

$$u_0^{(1)} = -\frac{r}{2} w_{0,z}^{(1)} \text{ and } u_0^{(2)} = -\frac{r}{2} w_{0,z}^{(2)}. \quad (28)$$

Integrating the radial momentum equation gives the pressures, namely,

$$p_0^{(1)} = -w_{0,z}^{(1)} + C_5(z,t), \tag{29}$$

$$p_0^{(2)} = -w_{0,z}^{(2)} + C_6(z,t). \tag{30}$$

Using the normal stress boundary conditions reveals that $C_5 = C_6 = 0$ and so

$$p_0^{(1)} = -w_{0,z}^{(1)} \text{ and } p_0^{(2)} = -w_{0,z}^{(2)}. \tag{31}$$

It remains to determine the axial velocity components and the evolutions of the free boundaries locating the radial extent of the fluids; we must go the next order to find these quantities.

Going to next order allows us to close the system. The leading order equations for the free surfaces and the leading order axial velocity component may be expressed in terms of the cross sectional areas as follows:

$$A_{1,t} + (A_1 w_0)_{,z} = 0, \tag{32}$$

$$A_{2,t} + (A_2 w_0)_{,z} = 0, \tag{33}$$

$$\frac{1}{a_1}\left[3(1-\mu_{12})A_1 w_{0,z}\right]_z + \frac{1}{a_2}\left[3\mu_{12}A_2 w_{0,z}\right]_z = 0. \tag{34}$$

Here the A_i with $i = 1, 2$ is the cross sectional area within a_1 and a_2 respectively; w_0 is the leading order axial velocity component that is a single function in both fluids.

3.2 Results

3.2.1 Numerics for two fluids

We tried a method of lines approach. We mapped the PDEs to a fixed domain with the variable $\zeta = z/L(t)$ so that in the new variable we have $0 \leq \zeta \leq 1$. We then applied centered finite difference methods on a uniform mesh for the spatial derivatives. The resulting system is differential-algebraic, though it was solved with essentially an ODE approach. The method first solved the algrebraic problem for axial velocity component w_{0j} for all j on the grid points and then solved the ODE's for the $a_{1j}(t)$ and $a_{2j}(t)$ at the grid points using either `ode45` or `ode15s` in Matlab. The code for the two fluid case is in Appendix B.

The initial conditions for computation are given by $A_1(\zeta, 0) = \delta_1 \sin(2\pi\zeta) + \bar{A}_1$ and $A_2(\zeta, 0) = \delta_2 \sin(2\pi\zeta) + \bar{A}_2$.

3.2.2 A first case

We begin with some sample computations where we chose $\mu_{12} = 2$, $\bar{A}_1 = 1$, $\bar{A}_2 = 1.5$ and $\delta_1 = \delta_2 = 0.1$; the results are shown in Figure 1. The left hand panel shows $A_i(\zeta, t)$, $i = 1, 2$, which is the total cross-sectional area within each fluid surface, as a function of space and time. The right hand panel compares the maximum and minimum values of the total cross-sectional area for each interface as a function of time. The subscripts are left off in the legend to reduce clutter; the lower curve in each case is for the inner interface located by A_1 and the upper curve is for the outer interface located by A_2. Note the logarithmic scales on each ordinate and the periodicity of the solution. There is a consistently a localized increase in amplitude with a relatively broad flat valley between. This strongly resembles the boudinage pictures from the geological papers, which justifies the original ansatz of the work. We now go on to vary the amplitude of the initial conditions and the viscosity ratio.

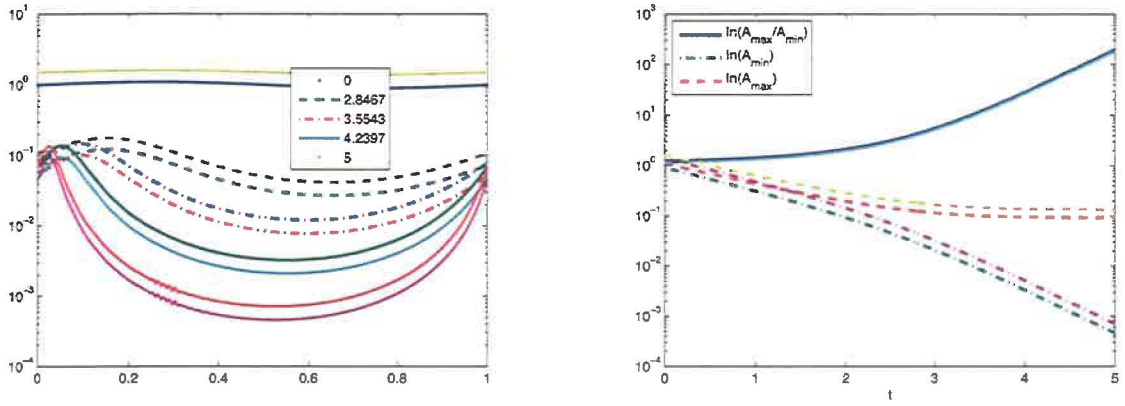

Figure 1: Left: Inner and total area as a function of ζ for different times. The nonlinearity in the instability is apparent. Right: Minimum and maximum film area, and their ratio, with time for $\mu_{12} = 2$, $\bar{A}_1 = 1$, $\bar{A}_2 = 1.5$ and $\delta_1 = \delta_2 = 0.1$. The maxima in the area appear to asymptote to a constant value. while the mimima appear to take on power law behavior (constant slope) at the latest times.

3.2.3 Varying the initial conditions

The rapidity with which the constant maximum area and the power law decrease in the minimum radii is obtained is accelerated when the initial disturbance amplitude is increased. Figure 2 shows results for a smaller disturbance amplitude and a slower development. Compare the results shown in Figure 1.

So far, the sinusoidal disturbances have been in phase. We now try the case when they are out of phase with $\mu_{12} = 2$, $\bar{A}_1 = 1$, $\bar{A}_2 = 1.5$ and $\delta_1 = -\delta_2 = 0.1$; results are shown in Figure 3. The maxima end up lining up anyway after an early adjustment period. The instability has been accelerated, with the minimum areas four to five times thinner in the out-of-phase case. The numerical instability is visible by $t = 4$ now, so it is encouraged in this case as well.

3.2.4 Changing the viscosity ratio

We now make a more viscous outer annulus compared to the core. We show results for $\mu_{12} = 5$, $\bar{A}_1 = 1$, $\bar{A}_2 = 1.5$ and $\delta_1 = \delta_2 = 0.1$ in Figure 4. These results develop much more slowly than for the smaller viscosity ratio for this in phase disturbance. For the out of phase disturbance with same high viscosity contrast, namely $\mu_{12} = 5$, $\bar{A}_1 = 1$, $\bar{A}_2 = 1.5$ and $\delta_1 = -\delta_2 = 0.1$ in Figure 5. In this case, the boudinage instability is promoted, with a large area contrast at the end time being observed. We don't yet know why the instability is promoted or retarded by these combinations in the nonlinear regime.

We now make the core 5 times more viscous than the outer layer, so that we compute for $\mu_{12} = 1/5$, $\bar{A}_1 = 1$, $\bar{A}_2 = 1.5$ and $\delta_1 = \delta_2 = 0.1$ in Figure 6. The boudinage instability is promoted in this case relative to the out of phase disturbance for the same parameters to follow, and although it is a little slower to develop, this case is similar to the $\mu_{12=5}$ case. For the out of phase case, we compute for $\mu_{12} = 1/5$, $\bar{A}_1 = 1$, $\bar{A}_2 = 1.5$ and $\delta_1 = \delta_2 = 0.1$ in Figure 7. In this case, the boudinage

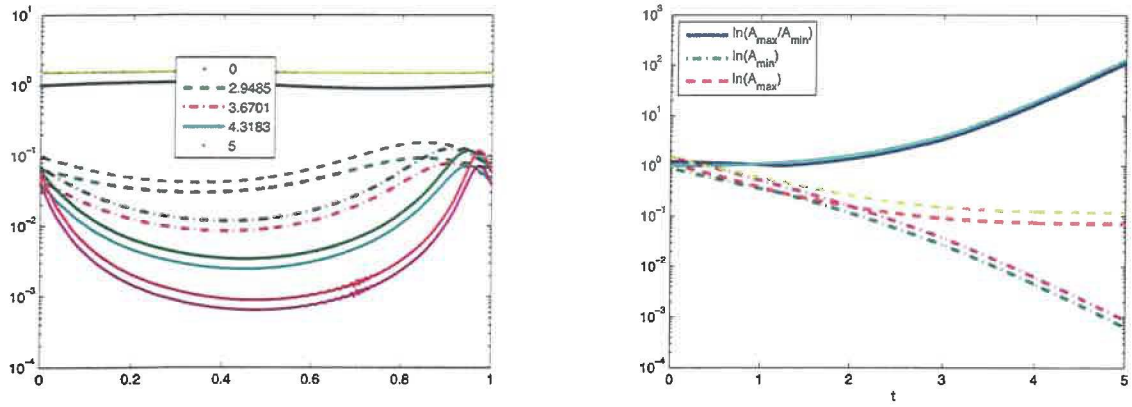

Figure 2: Left: Inner and total area as a function of ζ for different times. The nonlinearity in the instability develops more slowly with the smaller initial amplitude of the disturbance in the initial condition. Right: Minimum and maximum film area, and their ratio, with time for $\mu_{12} = 2$, $\bar{A}_1 = 1$, $\bar{A}_2 = 1.5$ and $\delta_1 = \delta_2 = 0.025$. It takes significantly longer to get to the late time behavior for the case when $\delta_1 = \delta_2 = 0.1$.

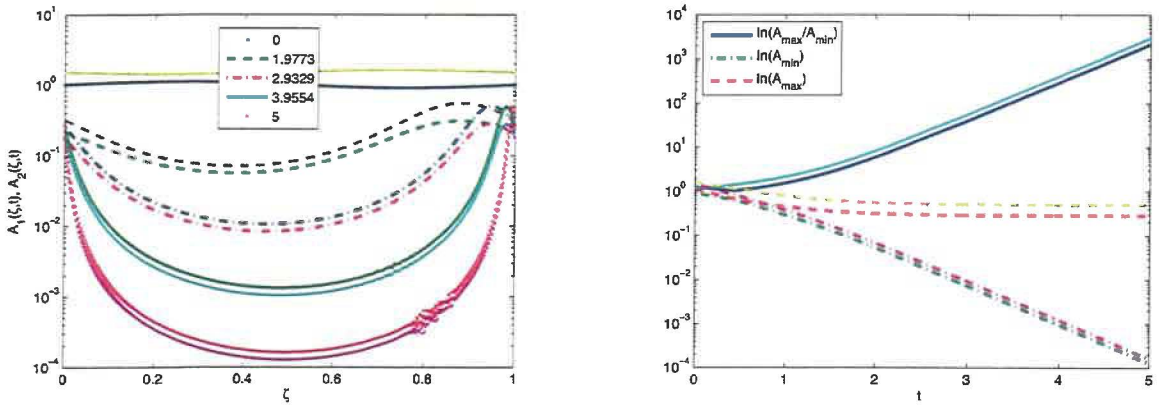

Figure 3: Left: Inner and total area as a function of ζ at different times for $\mu_{12} = 2$, $\bar{A}_1 = 1$, $\bar{A}_2 = 1.5$ and $\delta_1 = -\delta_2 = 0.1$; compare with in phase case shown in Figure 1. Right: Minimum and maximum film area, and their ratio, with time. The boudinage instability of the fiber is encouraged compared to the in-phase case.

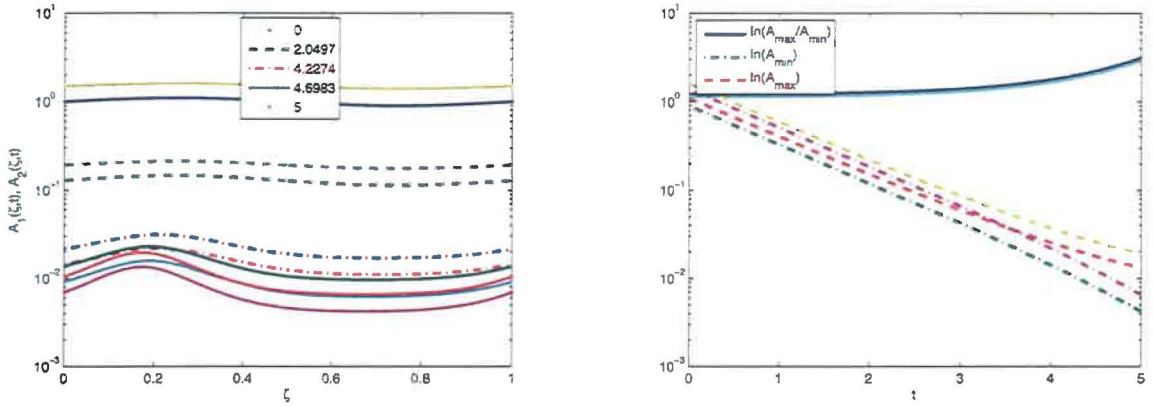

Figure 4: Left: Inner and total area as a function of ζ for different times for $\mu_{12} = 5$, $\bar{A}_1 = 1$, $\bar{A}_2 = 1.5$ and $\delta_1 = \delta_2 = 0.1$. The nonlinearity in the instability develops much more slowly with the increased viscosity contrast and an in-phase disturbance in the initial condition. Right: Minimum and maximum film area, and their ratio, with time. Note the small amplitude ratio at the last time.

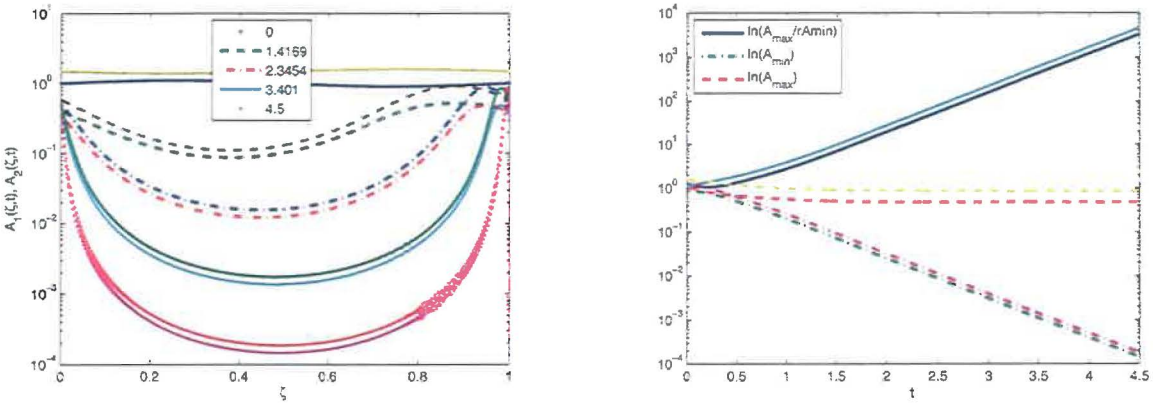

Figure 5: Left: Inner and total area as a function of ζ for different times for $\mu_{12} = 5$, $\bar{A}_1 = 1$, $\bar{A}_2 = 1.5$ and $\delta_1 = -\delta_2 = 0.1$. Here we have only integrated to $t = 4.5$ to avoid disastrous numerical instability. Right: Minimum and maximum film area, and their ratio, with time. Note the very large amplitude ratio at the last time; the instability from boudinage was promoted by the high viscosity ratio and out of phase disturbance.

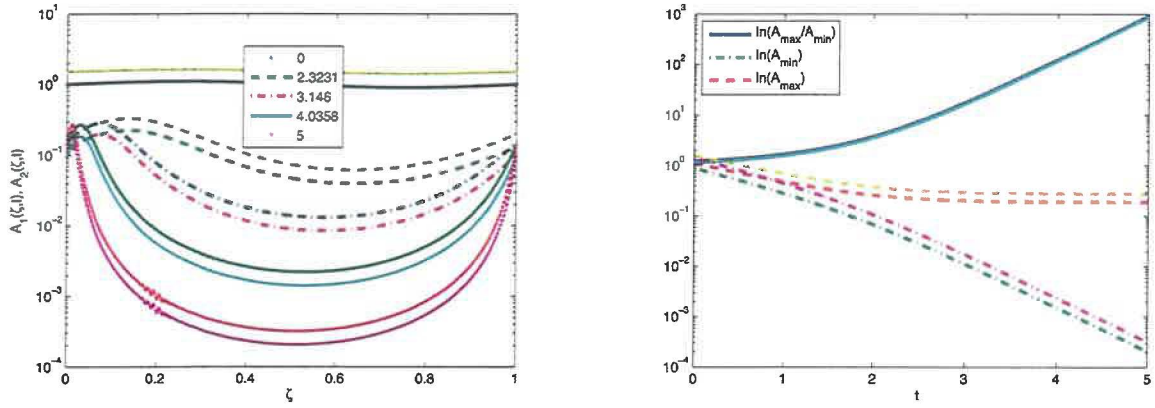

Figure 6: Left: Inner and total area as a function of ζ for different times for $\mu_{12} = 1/5$, $\bar{A}_1 = 1$, $\bar{A}_2 = 1.5$ and $\delta_1 = \delta_2 = 0.1$. Right: Minimum and maximum film area, and their ratio, with time. Note the very large amplitude ratio at the last time; the instability from boudinage was promoted by the high viscosity ratio and out of phase disturbance.

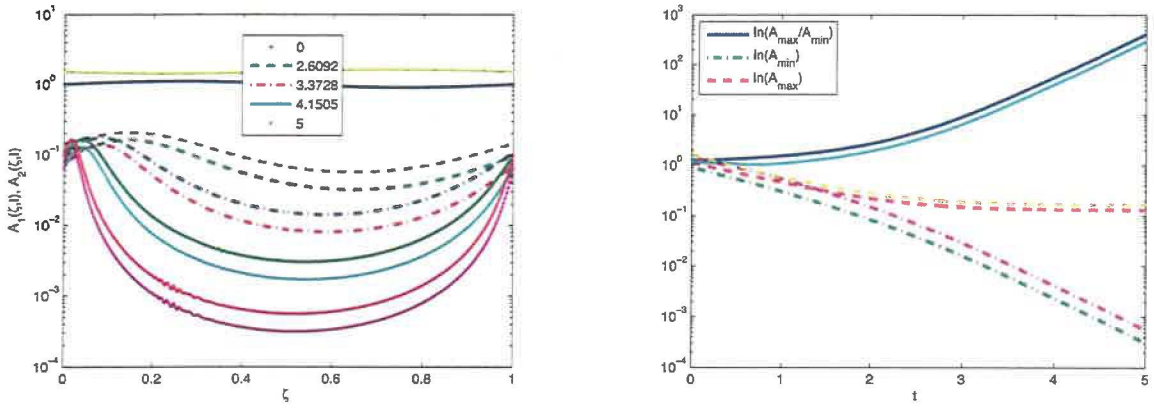

Figure 7: Left: Inner and outer thickness as a function of ζ for different times for $\mu_{12} = 1/5$, $\bar{A}_1 = 1$, $\bar{A}_2 = 1.5$ and $\delta_1 = -\delta_2 = 0.1$. Right: Minimum and maximum film thickness, and their ratio, with time. Note the smaller amplitude ratio at the last time; the instability from boudinage has been retarded by out of phase disturbance.

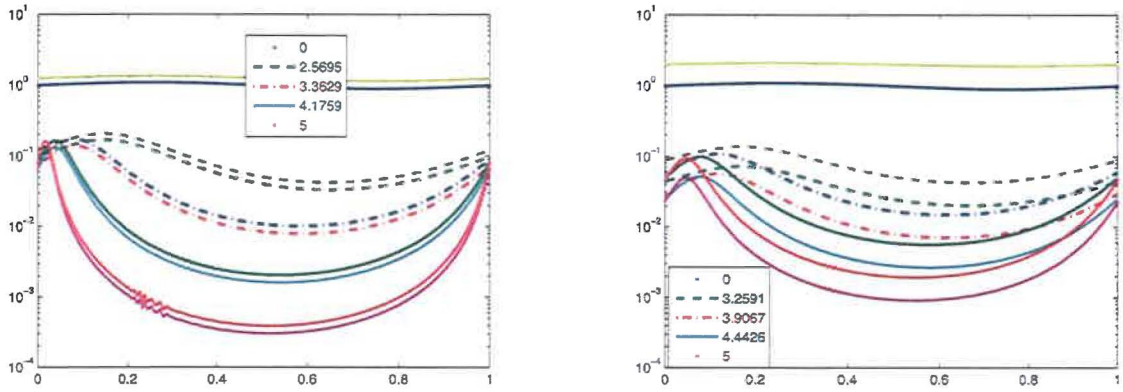

Figure 8: Inner and outer thickness as a function of ζ for different times. Left: $\bar{A}_2 = 1.25$; right: $\bar{A}_2 = 2$. The instability develops faster for smaller $\bar{A}_2$.

instability is retarded from the out of phase disturbance.

3.2.5 Numerical instability

Now for a bit more about the numerical instability. Making the initial conditions for the surface closer together promotes the numerical instability, while increasing the separation seems to less it. We show results for $\bar{A}_2 = 1.25$ and $\bar{A}_2 = 2$ with $\bar{A}_1 = 1$ and $\delta_1 = \delta_2 = 0.1$ as before in Figure 8 At this time we have not analyzed or fully understood the numerical instability.

3.2.6 Linear stability for two fluids

We now discuss the linear stability of the boudinage case with concentric fluids of different viscosity which was numerically solved in the previous section. We studied the class of perturbations for $L(t) = Vt$, that is, constant pulling speed and sinusoidal variation in the area. This corresponded to the numerical computations in the previous section. For the stability analysis is is convenient to put the equations on a fixed domain via the transformation $\zeta = z/L(t)$ as for the numerics; the equations are then

$$A_{1,t} - \frac{\dot{L}\zeta}{L} A_{1,\zeta} + (A_1 w_0)_{,\zeta} = 0, \tag{35}$$

$$A_{2,t} - \frac{\dot{L}\zeta}{L} A_{2,\zeta} + (A_2 w_0)_{,\zeta} = 0, \tag{36}$$

$$\frac{1}{a_1}\left[3(1-\mu_{12})A_1 w_{0,\zeta}\right]_\zeta + \frac{1}{a_2}\left[3\mu_{12} A_2 w_{0,\zeta}\right]_\zeta = 0. \tag{37}$$

We will make use of $L(t) = Vt$ where V is the constant stretch speed and we pose

$$A_1(\zeta, t) = \frac{V_1}{\pi V t}[1 + \delta \hat{A}_1(\zeta, t)], \tag{38}$$

$$A_2(\zeta,t) = \frac{V_2}{\pi V t}[1 + \delta \hat{A}_2(\zeta,t)], \tag{39}$$

$$w_0(\zeta,t) = V\zeta + \delta \hat{w}_0(\zeta,t), \tag{40}$$

where $\delta \ll 1$ is the perturbation amplitude and V_i is the volume inside the respective outer radii of the fluid.

Substituting the solution forms into the equations and linearizing gives, for the areas,

$$\hat{A}_{1,t} + \frac{\hat{w}_{0,\zeta}}{Vt} = 0, \tag{41}$$

$$\hat{A}_{2,t} + \frac{\hat{w}_{0,\zeta}}{Vt} = 0. \tag{42}$$

We can then use the last equation to solve for the quantity

$$\frac{\hat{w}_{0,\zeta}}{Vt} = -\frac{(V_1/V_2)^{3/2}(1-\mu_{12})\hat{A}_1 + \mu_{12}\hat{A}_2}{(V_1/V_2)^{3/2}(1-\mu_{12}) + \mu_{12}}\frac{1}{t} \tag{43}$$

Here we made use of

$$\frac{1}{\sqrt{A_i}} = \left(\frac{V_1}{\pi V t}\right)^{-1/2}(1 - \hat{A}_1\delta/2 + ...). \tag{44}$$

Solving for the area perturbation equation, we find

$$\tilde{A}_{1,t} = \tilde{A}_{2,t} = \frac{(V_1/V_2)^{3/2}(1-\mu_{12})\hat{A}_1 + \mu_{12}\hat{A}_2}{(V_1/V_2)^{3/2}(1-\mu_{12}) + \mu_{12}}\frac{1}{t}. \tag{45}$$

We now hypothesize sinusoidal disturbances in ζ, namely,

$$\hat{A}_i = \tilde{A}_i(t)\sin(k\pi\zeta), \quad i = 1,2; \tag{46}$$

substitution gives

$$\frac{d\tilde{A}_1}{dt} = \frac{d\tilde{A}_2}{dt} = \frac{(V_1/V_2)^{3/2}(1-\mu_{12})\hat{A}_1 + \mu_{12}\hat{A}_2}{(V_1/V_2)^{3/2}(1-\mu_{12}) + \mu_{12}}\frac{1}{t}. \tag{47}$$

We can see that the initial change in the size of the amplitude of the perturbations depends on the size of the perturbations, the viscosity contrast between the different materials and the phase of the disturbances (i.e., the sign of the disturbance amplitudes). However, trends are not immediately apparent.

Suppose that we now wish to make the phase of the disturbances explicit; we choose $\tilde{A}_2 = \pm|\tilde{A}_2|$ and then find

$$\frac{d\tilde{A}_1}{dt} = \pm\frac{d|\tilde{A}_2|}{dt} = \frac{(V_1/V_2)^{3/2}(1-\mu_{12})\hat{A}_1 + \mu_{12}(\pm|\hat{A}_2|)}{(V_1/V_2)^{3/2}(1-\mu_{12}) + \mu_{12}}\frac{1}{t}. \tag{48}$$

The sign change between the two areas for the initial change may explain why the out of phase case (minus sign) decays and then the in phase shape appears during the nonlinear evolution.

3.3 Discussion

We've explored the stretching in the two fluid case, and only considered the effect of differing viscosities in an inclusion. The case with an out-of-phase disturbance and a less viscous core seemed to be the most unstable, showing a ratio of maximum to minimum approaching 10^4 is when integrating to $t = 5$. This extreme value is reminiscent of the extreme instability shown in Smith [25] in geologic formations. At such extreme values, it is reasonable to expect that other physics may be needed, e.g., surface tension and inertia.

The idea that a boudinage-type instability may occur and contribute in fiber pulling appears to be a good one.

4 Conclusion

Remaining tasks for the future are manifold. A critical extension is to the three-fluid case. The inclusion of gravity, inertia, surface tension and non-Newtonian effects on the boundinage/mullions instability would be of interest. This is certainly accessible given appropriate time.

Another direction is to consider the effect of thermal perturbations on the pulling when there is taper in the drawn fiber.

References

[1] J. Abbott, P. Howell, C.P. Please, et al. "Boundary Layers and Material Deformation in Fiber Drawaing," in *Proceedings of the 2001 Mathematical Problems in Industry Workshop*, (40 pp.).

[2] P.D. Howell, "Extensional Thin Layer Flows," D.Phil. Thesis, U. Oxford (1994).

[3] J.R.A. Pearson and M.A. Matovich, "Spinning a Molten Threadline," *Ind. Eng. Chem. Fund.* (1969) **8**(4):605-609.

[4] W.W. Schultz and S.H. Davis, "Effects of Boundary Conditions on the Stability of Slender Viscous Fibers," *J. Appl. Mech.*, (1984) **106**:1-5.

[5] F.T. Geyling and Homsy, "Extensional Instabilities of the Glass Fiber Drawing Process," *Glass Tech.*, (1980) **21**:95-102.

[6] D. Gelder, "On Stability of the Fiber Drawing Process," *Ind. Eng. Chem. Fund.* (1971) **10**(3):534-535.

[7] J.C. Chang, M.M. Denn and F.T. Geyling, "Effects of Intertial, Surface Sension, and Gravity on the Stability of Isothermal Fiber Spinning," *Ind. Eng. Chem. Fund.* (1981) **20**(2):147-149.

[8] J.R.A. Pearson *Mechanics of Polymer Processing*, (Elsevier, London, 1985) Ch. 15.

[9] Y.T. Shah and J.R.A. Pearson, "On the Stability of Nonisothermal Fiber Spinning," *Ind. Eng. Chem. Fund.* (1972) **11**(2):145-149.

[10] Y.T. Shah and J.R.A. Pearson, "On the Stability of Nonisothermal Fiber Spinning–General Case," *Ind. Eng. Chem. Fund.* (1972) **11**(2):150-153.

[11] G.H. Gupta, W.W. Schultz, E.M. Arruda and X. Lu, "Nonisothermal Model of Glass Fiber Stability," *Rheol. Acta*, (1996) **35**:584-596.

[12] C. Voyce, D.Phil. Thesis, U. Southampton, 2006.

[13] S.H. Law, G.W. Barton, T.N. Phan and M.J. Barton, "The interpretation of online measurements of optical fiber diameter", *Trans. Inst. Measurement and Control* (2005) **27**:215-229.

[14] S.H. Law, G.W. Barton, et al., "The Causes and Nature of Diameter Variations Along Optical Fiber," *Micro- and Nanotechnology. Proc. SPIE*, (2005) **5650**:23-34

[15] F. Onofri, A. Lenoble, S. Radev and P-H. Guering, "High Resolution monitoring of an unsteady glass fibre drawing process", *Exp. Fluids* (2007) **42**:601-610.

[16] G.W. Barton, S.H. Law and T.N. Phan, "Limitations to the Manufacture of Specialty Optical Fiber," *ASME J. Manuf. Sci. Eng.* (2005) **127**:663-669.

[17] Cheng and Jaluria, "Feasibility of High Speed Furnace Drawing of Optical Fibers," *ASME J. Heat Transfer*, (2004) **126**:852-857.

[18] C. Voyce, private communication (2007).

[19] A.L. Yarin, P. Gospodinov, O. Gottlieb and M.D. Graham, "Newtonian glass fiber drawing: Chaotic variation of the cross-sectional radius", *Phys. Fluids* (1999) **11**(11):3201-3208.

[20] P. Gospodinov and A.L. Yarin, "Draw Resonance of Optical Microcapillaries in Non-isothermal Drawing," *Int. J. Multiphase Flow*, (1997) **23**(5):967-976.

[21] A.D. Fitt, K. Furusawa, T.M. Monro and C.P. Please, "Modelling the fabrication of hollow fibers: capillary drawing," *J. Lightwave Tech.*, (2001) **31**:1924-1931.

[22] A.D. Fitt, K. Furusawa, T.M. Monro, C.P. Please and D.J. Richardson, "The mathematical modelling of capillary drawing for holey fibre manufacture," *J. Eng. Math.*, (2002) **31**:201-227.

[23] Pone et al., "Drawing of the hollow all-polymer Bragg fibers", *Optics Express*, (2006) **14**(13):5838-5852.

[24] C. Chen and Y. Jaluria, "Numerical Simulation of Transport in Optical Fiber Drawing with Core-Cladding Structure," *ASME J. Heat Transfer*, (2007) **129**:559-567.

[25] R.B. Smith, "Unified Theory of the Onset of Folding, Boudinage and Mullion Structure," *Geol. Soc. Am. Bull.*, (1975) **86**:1601-1609.

[26] R.B. Smith, "Formation of Folds, Boudinage and Mullions in non-Newtonian Materials," *Geol. Soc. Am. Bull.*, (1977) **88**:312-320.

[27] Spence and Sharp, "Distortion and necking of a viscous inclusion in Stokes flow," *Proc. Roy. Soc. A* (1989) **422**:173-192.

[28] Spence, Ockendon, Wilmott, Turcotte, Kellogg, "Convective mixing in the mantle: The role of viscosity," *Geophysical J.*, (1988) **95**:79-86.

[29] N.C. Gay, "Pure Shear and Simple Shear Deformation of Inhomogeneous Viscous Fluids. 1. Theory: Tectonophyscis," (1968) 5:211-234.

[30] Paek and Runk, "Physical behaviour of the neck-down region during furnace drawing of silica fibers", J. Appl. Phys. 49 (1978) pp.4417-4422.

Appendix A: Nonlinear and linearized problem in terms of radii

In case it is useful, the problems in terms of radii for two-fluid Boudinage are given here. We first record the eq In terms of the radii $a_i(z,t)$ with $i = 1, 2$, we may write the equations as follows:

$$2a_1 a_{1,t} + (a_1^2 w_0)_{,z} = 0, \tag{49}$$

$$2a_2 a_{2,t} + (a_2^2 w_0)_{,z} = 0, \tag{50}$$

$$\frac{1}{a_1}\left[3(1-\mu_{12})a_1^2 w_{0,z}\right]_z + \frac{1}{a_2}\left[3\mu_{12} a_2^2 w_{0,z}\right]_z = 0. \tag{51}$$

The boundary conditions are again $w_0(0,t) = 0$, $w(L,t) = \dot{L}$ with periodicity in the a_i.

A z-independent solution is available for the radii, namely

$$\bar{a}_1(t) = \sqrt{\frac{V_1}{\pi L(t)}}, \qquad \text{with } \bar{a}_1(0) = \sqrt{\frac{V_1}{\pi L(0)}} = R_{10}, \tag{52}$$

$$\bar{a}_2(t) = \sqrt{\frac{V_2}{\pi L(t)}}, \qquad \text{with } \bar{a}_2(0) = \sqrt{\frac{V_2}{\pi L(0)}} = R_{20}, \tag{53}$$

$$\bar{w}_0(z,t) = \frac{\dot{L}}{L} z. \tag{54}$$

Here we have made use of cylindrical geometry at all times where $V_i(t) = \pi L(t)[a_i(t)]^2$, with $i = 1, 2$.

Applying the perturbations

$$a_1(z,t) = \bar{a}_1(t) + \delta\hat{a}_1(z,t) \tag{55}$$

$$a_2(z,t) = \bar{a}_2(t) + \delta\hat{a}_2(z,t) \tag{56}$$

$$w_0(z,t) = \bar{w}_0(t) + \delta\hat{w}_0(z,t) \tag{57}$$

and linearizing gives the linear stability problem as follows:

$$2(\bar{a}_1\hat{a}_{1,t} + \hat{a}_1\bar{a}_{1,t}) + \left[2\bar{a}_1\hat{a}_1\bar{w}_0 + (\bar{a}_1)^2\hat{w}_0\right]_{,z} = 0, \tag{58}$$

$$2(\bar{a}_2\hat{a}_{2,t} + \hat{a}_2\bar{a}_{2,t}) + \left[2\bar{a}_2\hat{a}_2\bar{w}_0 + (\bar{a}_2)^2\hat{w}_0\right]_{,z} = 0, \tag{59}$$

$$\frac{1}{\bar{a}_1}\left[3(1-\mu_{12})(2\bar{a}_1\hat{a}_1\bar{w}_{0,z} + (\bar{a}_1)^2\hat{w}_{0,z})\right]_z + \frac{1}{\bar{a}_2}\left[3\mu_{12}(2\bar{a}_2\hat{a}_2\bar{w}_{0,z} + (\bar{a}_2)^2\hat{w}_{0,z})\right]_z = 0. \tag{60}$$

It is convenient for analysis to choose $L(t) = Vt$ so that we pull with constant speed; then $\bar{w}_0 = Vz$ and $\hat{w}_0(0,t) = \hat{w}_0(L,t) = 0$ corresponds to no perturbation to the pulling speed, and the radii are initially sinusoidal.

Appendix B: Code for single fluid case

```
function [t,z,y] = onefluid1(N,tout,imethod,Amean,Ainit)
% function [t,z,y] = onefluid1(N,tout,imethod,Amean,Ainit)
%
% one fluid code for Corning problem
% uses either ode45 or ode15s with finite difference MOL
%     manually solves for algebraic variable, so really solving odes
% Input
%   N = total number of grid points (including ends)
%   tout = final time
%   imethod = 1 for ode45, 2 for ode15s
%   Amean = initial mean area
%   Ainit = amplitude of initial inner area perturbation
%   Binit = amplitude of initial total area perturbation
% Output
%   t = output times
%   z = spatial mesh
%   u = dependent variable solution; each row is a different time
%         and 1:N is A

% N = 201; %number of total node points
z = linspace(0,1,N);

A = Ainit*sin(2*pi*z)+Amean; % Initial State

% Boundary conditions
w0 = 0;
wL = 1;

options = odeset('RelTol',1e-6,'AbsTol',1e-6);
if (imethod==1)
    [t,y]= ode45(@timeDer,[0 tout],A,options,w0,wL,N);
else
    [t,y]= ode15s(@timeDer,[0 tout],A,options,w0,wL,N);
end
%surf(y)
%keyboard
%hold off
figure;
for i = 1:length(t)
    plot3(diag(t(i)*eye(N)),z, y(i,1:N)*(t(i)+1));
    hold on
end
ymin = (min(y'))';
ymax = (max(y'))';
```

```
yrat = ymax./ymin;
figure
semilogy(t,yrat,'-',t,ymin,'-.',t,ymax,'--','LineWidth',2);
xlabel('t');
legend('ln(r_{max}/r_{min})','ln(r_{min})','ln(r_{max})',2);
figure;
i1 = round(length(t)/4);
i2 = round(length(t)/2);
i3 = round(length(t)*3/4);
semilogy(z,y(1,:),'.',z,y(i1,:),'--',z,y(i2,:),'-.',z,y(i3,:),'-',z,y(end,:),'.');
legend(gca,num2str(t(1)),num2str(t(i1)),num2str(t(i2)),num2str(t(i3)),num2str(t(end)),1);

end

%keyboard

function Adot = timeDer(t,A,w0,wL,N)

% Finite difference implementation to compute w

z = linspace(0,1,N);
delZ = z(2)-z(1);
W(1:N) = w0;
W(N) = wL;

Mat = zeros(N-2,N-2);
RHS = zeros(N-2,1);

Mat(1,1) = -(A(3)+2*A(2)+A(1)); % N = 2
Mat(1,2) = A(3)+A(2);
RHS(1,1) = -(A(2)+A(1))*W(1);

Mat(N-2,N-3) = A(N-1)+A(N-2);  % N = N-1
Mat(N-2,N-2) = -(A(N)+2*A(N-1)+A(N-2));
RHS(N-2,1) = -(A(N)+A(N-1))*W(N);

nodeID = 3;
for i = 1:N-4
    Mat(i+1,i) = A(nodeID)+A(nodeID-1);
    Mat(i+1,i+1) = -(A(nodeID+1)+2*A(nodeID)+A(nodeID-1));
    Mat(i+1,i+2) = A(nodeID+1)+A(nodeID);
    nodeID = nodeID+1;
end

Wsol(2:N-1) = Mat\RHS;
```

```
Wsol(1) = W(1); % wL
Wsol(N) = W(N); % wR

% To compute Adot
Ldot = 1;
L = 1;
%
% for i = 1:N-1
%     Adot(i) = (Ldot/L)*(i-1)*(A(i+1)-A(i)) - ...
                (A(i)*(Wsol(i+1)-Wsol(i))+Wsol(i)*(A(i+1)-A(i)))/(L*delZ) ;
% end
% Adot(N) = (Ldot/L)*(N-1)*(A(i)-A(i-1)) - ...
              (A(i)*(Wsol(i)-Wsol(i-1))+Wsol(i)*(A(i)-A(i-1)))/(L*delZ) ;
% Adot = Adot';

for i = 2:N-1
    Adot(i,1) = -(Wsol(i+1)*A(i+1) - Wsol(i-1)*A(i-1))/(2*delZ*L) +...
                  z(i)*Ldot*(A(i+1)-A(i-1))/(2*delZ*L);
end
Adot(1,1) = -A(1)*(-Wsol(3)+4*Wsol(2)-3*Wsol(1))/(2*delZ*L);
Adot(N,1) = -A(N)*(3*Wsol(N)-4*Wsol(N-1)+Wsol(N-2))/(2*delZ*L);

end
```

Appendix C: Code for two fluid case

```
function [t,z,y] = twofluid1(N,tout,imethod,Amean,Bmean,Ainit,Binit,visrat)
% function [t,z,y] = twofluid1(N,tout,imethod,Ainit,Binit)
%
% two fluid code for Corning problem
% uses either ode45 or ode15s with finite difference MOL
%     manually solves for algebraic variable, so really solving odes
% Input
%   N = total number of grid points (including ends)
%   tout = final time
%   imethod = 1 for ode45, 2 for ode15s
%   Amean = initial inner mean area
%   Bmean = initial total mean area
%   Ainit = amplitude of initial inner area perturbation
%   Binit = amplitude of initial total area perturbation
%   visrat = viscosity ratio (outer/inner)
% Output
%   t = output times
%   z = spatial mesh
%   y = dependent variable solution; each row is a different time
%         and 1:N is A, N+1:2*N is B

%N = 201; %total number of node points
z = linspace(0,1,N);

A = Ainit*sin(2*pi*z)+Amean; % Initial State
B = Binit*sin(2*pi*z)+Bmean; % Initial State
% Boundary conditions
w0 = 0;
wL = 1;
statevec = [A,B]';
options = odeset('RelTol',1e-6,'AbsTol',1e-6);
if (imethod == 1)
    [t,y]= ode45(@timeDer,[0 tout],statevec,options,w0,wL,N,visrat);
else
    [t,y]= ode15s(@timeDer,[0 tout],statevec,options,w0,wL,N,visrat);
end
%figure
%surf(y(:,1:N));
%hold on
%surf(y(:,N+1:2*N));
hold off
figure
waterfall(y(:,1:N));
```

```
figure
for i = 1:10:length(t)
    plot3(diag(t(i)*eye(N)),z, y(i,1:N)*(t(i)+1));
    hold on
    plot3(diag(t(i)*eye(N)),z,y(i,N+1:2*N)*(t(i)+1));
end

figure
yinmin = (min(y(:,1:N)'))';
yinmax = (max(y(:,1:N)'))';
youtmin = (min(y(:,N+1:2*N)'))';
youtmax = (max(y(:,N+1:2*N)'))';
yinrat = yinmax./yinmin;
youtrat = youtmax./youtmin;
semilogy(t,yinrat,'-',t,yinmin,'-.',t,yinmax,'--',t,youtrat,'-',...
         t,youtmin,'-.',t,youtmax,'--','LineWidth',2);
xlabel('t');
legend('ln(r_{max}/r_{min})','ln(r_{min})','ln(r_{max})',2);

figure
i1 = round(length(t)/4);
i2 = round(length(t)/2);
i3 = round(length(t)*3/4);
semilogy(z,y(1,1:N),'.',z,y(i1,1:N),'--',z,y(i2,1:N),'-.',z,y(i3,1:N),'-',...
     z,y(end,1:N),'.',z,y(1,N+1:2*N),'.',z,y(i1,N+1:2*N),'--',z,y(i2,N+1:2*N),...
     '-.',z,y(i3,N+1:2*N),'-',z,y(end,N+1:2*N),'.',...
    'LineWidth',2);
legend(gca,num2str(t(1)),num2str(t(i1)),num2str(t(i2)),num2str(t(i3)),num2str(t(end)),3);
xlabel('\zeta'); ylabel('A_1(\zeta,t), A_2(\zeta,t)');

% keyboard

function Dotvec = timeDer(t,statevec,w0,wL,N,Mu)

%the A and B are areas, not radii.
A = statevec(1:N,1);
B = statevec(N+1:2*N,1);
%Mu = 2;

% Finite difference implementation to compute w

z = linspace(0,1,N);
delZ = z(2)-z(1);
W(1:N) = w0;
W(N) = wL;
```

```
Mat = zeros(N-2,N-2);
RHS = zeros(N-2,1);

Mat(1,1) = -(A(3)+2*A(2)+A(1))*(1-Mu)/sqrt(A(2)) -...
             (B(3)+2*B(2)+B(1))*Mu/sqrt(B(2)) ; % N = 2
Mat(1,2) = (A(3)+A(2))*(1-Mu)/sqrt(A(2)) + (B(3)+B(2))*Mu/sqrt(B(2));
RHS(1,1) = -(A(2)+A(1))*W(1)*(1-Mu)/sqrt(A(2)) -(B(2)+B(1))*W(1)*Mu/sqrt(B(2));

Mat(N-2,N-3) = (A(N-1)+A(N-2))*(1-Mu)/sqrt(A(N-1)) + ...
               (B(N-1)+B(N-2))*Mu/sqrt(B(N-1))  ;  % N = N-1
Mat(N-2,N-2) = -(A(N)+2*A(N-1)+A(N-2))*(1-Mu)/sqrt(A(N-1))-...
                (B(N)+2*B(N-1)+B(N-2))*Mu/sqrt(B(N-1));
RHS(N-2,1) = -(A(N)+A(N-1))*W(N)*(1-Mu)/sqrt(A(N-1))-...
              (B(N)+B(N-1))*W(N)*Mu/sqrt(B(N-1))  ;

nodeID = 3;
for i = 1:N-4
    Mat(i+1,i) = (A(nodeID)+A(nodeID-1))*(1-Mu)/sqrt(A(nodeID))+...
                  (B(nodeID)+B(nodeID-1))*Mu/sqrt(B(nodeID))  ;
    Mat(i+1,i+1) = -(A(nodeID+1)+2*A(nodeID)+A(nodeID-1))*(1-Mu)/sqrt(A(nodeID))-...
                  (B(nodeID+1)+2*B(nodeID)+B(nodeID-1))*Mu/sqrt(B(nodeID));
    Mat(i+1,i+2) = (A(nodeID+1)+A(nodeID))*(1-Mu)/sqrt(A(nodeID))+...
                  (B(nodeID+1)+B(nodeID))*Mu/sqrt(B(nodeID));
    nodeID = nodeID+1;
end

Wsol(2:N-1) = Mat\RHS;
Wsol(1) = W(1); % wL
Wsol(N) = W(N); % wR

% To compute Adot and Bdot
Ldot = 1;
L = 1;

% for i = 1:N-1
%     Adot(i,1) = (Ldot/L)*(i-1)*(A(i+1)-A(i)) - ...
%                  (A(i)*(Wsol(i+1)-Wsol(i))+Wsol(i)*(A(i+1)-A(i)))/(L*delZ) ;
%     Bdot(i,1) = (Ldot/L)*(i-1)*(B(i+1)-B(i)) - ...
%                  (B(i)*(Wsol(i+1)-Wsol(i))+Wsol(i)*(B(i+1)-B(i)))/(L*delZ);
% end
i = 1;
Adot(1,1) = (Ldot/L)*(i-1)*(A(i+1)-A(i)) - ...
             (A(i)*(Wsol(i+1)-Wsol(i))+Wsol(i)*(A(i+1)-A(i)))/(L*delZ) ;
Bdot(1,1) = (Ldot/L)*(i-1)*(B(i+1)-B(i)) - ...
```

```
            (B(i)*(Wsol(i+1)-Wsol(i))+Wsol(i)*(B(i+1)-B(i)))/(L*delZ);
i = N;
Adot(N,1) = (Ldot/L)*(N-1)*(A(i)-A(i-1)) - ...
             (A(i)*(Wsol(i)-Wsol(i-1))+Wsol(i)*(A(i)-A(i-1)))/(L*delZ) ;
Bdot(N,1) = (Ldot/L)*(N-1)*(B(i)-B(i-1)) - ...
             (B(i)*(Wsol(i)-Wsol(i-1))+Wsol(i)*(B(i)-B(i-1)))/(L*delZ) ;

for i = 2:N-1
    Adot(i,1) = -(Wsol(i+1)*A(i+1) - Wsol(i-1)*A(i-1))/(2*delZ*L) + ...
                  z(i)*Ldot*(A(i+1)-A(i-1))/(2*delZ*L);
    Bdot(i,1) = -(Wsol(i+1)*B(i+1) - Wsol(i-1)*B(i-1))/(2*delZ*L) + ...
                  z(i)*Ldot*(B(i+1)-B(i-1))/(2*delZ*L);
end
% Adot(1,1) = -A(1)*(-Wsol(3)+4*Wsol(2)-3*Wsol(1))/(2*delZ*L);
% Bdot(1,1) = -B(1)*(-Wsol(3)+4*Wsol(2)-3*Wsol(1))/(2*delZ*L);
%
% Adot(N,1) = -A(N)*(3*Wsol(N)-4*Wsol(N-1)+Wsol(N-2))/(2*delZ*L);
% Bdot(N,1) = -B(N)*(3*Wsol(N)-4*Wsol(N-1)+Wsol(N-2))/(2*delZ*L);

Dotvec = [Adot;Bdot];
```